



# Effect of alkaline and atom-planting treatment on the catalytic performance of ZSM-5 catalyst in pyridine and picolines synthesis

Fang Jin<sup>a,b</sup>, Yugang Cui<sup>a</sup>, Yongdan Li<sup>a,\*</sup>

<sup>a</sup>Tianjin Key Laboratory of Applied Catalysis Science and Technology, School of Chemical Engineering, Tianjin University, Weijin Road 92, Tianjin 300072, China

<sup>b</sup>Key Laboratory for Green Chemical Process of Ministry of Education, School of Chemical and Pharmaceutical Engineering, Wuhan Institute of Technology, Wuhan 430073, China

## ARTICLE INFO

### Article history:

Received 14 May 2008

Received in revised form 28 July 2008

Accepted 31 July 2008

Available online 7 August 2008

### Keywords:

ZSM-5

Pyridine base

Desilication

Hierarchical pore

Galliation

## ABSTRACT

For the gas phase synthesis of pyridine and picolines, a successive alkaline and atom-planting treatment was employed to tailor the H-ZSM-5, and a catalyst containing hierarchical pore and framework Ga cations was prepared. Desilication was the major consequence of the alkaline treatment, while a slight dealumination happened simultaneously. A large number of meso- and macropores were introduced into the H-ZSM-5. The generated silanol groups, formed octahedral aluminum and decreased zeolite framework Si/Al caused decrease of the strong acid sites and increase of the weak acid sites and Lewis/Brönsted (L/B) ratio. Subsequent atom-planting treatment consumed the silanol groups and generated the bridged hydroxyl groups Si(OH)Ga, which resulted in decrease of the L/B ratio and the weak acid sites and increase of the strong acid sites. The catalytic performance shows that the introduced hierarchical pores increased the stability of the catalysts. The pyridine bases yield were not influenced by the generation of silanol groups and weak acid sites, while they were increased by the generation of Si(OH)Ga. The change of the P/3P has the same trend as that of L/B. The coke-introduced selectivation caused the gradual increase of P/3P during the deactivation of the original H-ZSM-5.

© 2008 Elsevier B.V. All rights reserved.

## 1. Introduction

Pyridine bases, i.e. pyridine and picolines, are the key important family of heterocyclic compounds for the production of various intermediates of pharmaceutical, agricultural, and other fine chemicals. Chichibabin first achieved the synthesis of pyridine bases from aldehyde, diethylformal and ammonia on alumina at 643 K in 1924 [1]. Since then the vapor phase synthesis of pyridine bases from different type aldehydes has been widely applied to industrial process in fixed or fluidized bed reactors of Reilly, Mobil, ICI, BASF, Koei Chemicals and others companies [2–10]. Chichibabin condensation of formaldehyde, acetaldehyde and ammonia, which are the cheap and handy raw materials, has provided a good prospect to meet the growing demand for pyridine, 2-picoline and 3-picoline. ZSM-5 zeolite has intrinsic acidity, three-dimensional porosity and capability to incorporation of trivalent cations other than Al in framework, and therefore, has been explored extensively

as a catalyst for the Chichibabin reaction in recent years [9–15]. The activity of the catalyst is sensitive to its acidity [12,16]. However, the intracrystalline diffusion limitation in micropore of ZSM-5 results in heavy coking and deactivation of the catalyst [12,13].

The diffusion limitation in the micropore of zeolite can be minimized by introducing the extra-pores [17,18]. Recently, alkaline treatment has been explored as an effective approach to create extra-pores in high silica zeolites, such as ZSM-5 [18–25]. The acidity of ZSM-5 zeolite can be modified by incorporating trivalent cations into the framework sites using the atom-planting method [26–30]. By this method, the metallosilicates can be prepared by the gas–solid reaction of the corresponding metal chloride vapor with siliceous zeolites. The reactivity of this gas–solid reaction depends on the concentration of zeolite defect sites, which are the four internal silanol groups [26–29,31].

In this paper, a combined method of successive alkaline and atom-planting treatment was explored on a commercial H-ZSM-5 zeolite in order to develop hierarchical pore and modify acidity. The objective is to prepare a tailored zeolite catalyst with an improved stability and activity in the Chichibabin condensation of formaldehyde, acetaldehyde and ammonia for pyridine and picolines synthesis.

\* Corresponding author at: Tianjin Key Laboratory of Applied Catalysis Science and Technology, School of Chemical Engineering, Tianjin University, Weijin Road 92, Tianjin 300072, China. Tel.: +86 22 27405613; fax: +86 22 27405243.

E-mail address: [ydli@tju.edu.cn](mailto:ydli@tju.edu.cn) (Y.D. Li).

## 2. Experimental

### 2.1. Catalyst samples

The original ZSM-5 zeolite was supplied by Nanlian Institute of Sinopec Jinling Petrochemical Corporation. The sample was calcined at 823 K for 5 h according to the guidelines of the manufacturer to convert it to H form. The parent sample was designated as H-ZSM-P.

For alkaline treatment, H-ZSM-P was stirred in 0.2 M NaOH solution at 338 K for 0.5 h, 1 g zeolite in 30 ml solution. The slurry was then cooled down with an ice bath and filtrated. The filtration cake was washed with deionized water until pH 7 was reached, and the cake was dried at 383 K. After the alkaline treatment Na form sample was obtained. It was ion-exchanged with 1 M  $\text{NH}_4\text{NO}_3$  solution, 1 g zeolite in 50 ml, and stirred at 298 K in a flask for 8 h, the slurry was filtrated and washed with deionized water, then the filtration cake was dried at 383 K. The ion-exchange and wash-filtration-drying steps were repeated for 3 times. The H form, named as H-ZSM-At, was obtained by calcination at 823 K for 5 h.

For the atom-planting treatment, a 4 g H-ZSM-At sample was placed in a quartz tube reactor and swept for 4 h at 723 K in a stream of purified and dried  $\text{N}_2$  with a flow rate  $70 \text{ ml min}^{-1}$  (STP). Then the reactor was brought to the reaction temperature 873 K. The  $\text{N}_2$  was saturated with anhydrous  $\text{GaCl}_3$  vapors at 403 K and passed through the samples in the reactor for 5 h with a flow rate  $50 \text{ ml min}^{-1}$  (STP). After completion of the reaction the sample was purged with  $\text{N}_2$  at 873 K for 3 h to remove unreacted the  $\text{GaCl}_3$  and then cooled down in the  $\text{N}_2$  stream. After that the sample was washed with a large amount of deionized water until the filtrate achieved pH value as 7, and then dried at 383 K. The sample was transformed into the  $\text{NH}_4^+$  form by ion-exchange with  $\text{NH}_4\text{NO}_3$  solution, and the wash-filtration-drying steps were repeated for 3 times. The H form, named as H-ZSM-At-Ga, was obtained by calcination at 823 K for 5 h.

### 2.2. Characterization

Powder X-ray diffraction (XRD) was performed using a Panalytical X'Pert automatic diffractometer with a  $\text{CoK}\alpha$  radiation. Solid-state  $^{27}\text{Al}$  and  $^{29}\text{Si}$  NMR spectra were collected with a Varian Infinity plus 300 WB spectrometer.  $^{27}\text{Al}$  spectra were obtained at 78.1 MHz, with a pulse width of 0.6  $\mu\text{s}$ , a pulse delay of 20 s, a spinning rate of 4 kHz.  $^{29}\text{Si}$  spectra were recorded at 59.6 MHz, with a pulse width of 5  $\mu\text{s}$ , a pulse delay of 15 s, a spinning rate of 4 kHz. The  $^1\text{H}$ - $^{29}\text{Si}$  cross-polarization (CP) MAS NMR spectra was also recorded on the same spectrometer. A contact time of 3 ms was used to enhance selectively the silanol group signals. The OXFORD ISIS300 EDX was used to analyze the atomic percentage of Ga on the samples.

$\text{N}_2$  adsorption and desorption isotherms were measured at 77 K on a QuadraSorb SI gas sorption analyzer after a vacuum pretreatment at 473 K for 8 h. Total specific surface areas ( $S_{\text{BET}}$ ) were calculated using the BET method [32], whereas total pore volume ( $v_{\text{total}}$ ) was evaluated from  $\text{N}_2$  uptake at a relative pressure of  $\text{N}_2$  equal to 0.99. The  $t$ -plot was employed to evaluate the volume of micropore ( $v_{\text{micropore}}$ ) and the total surface area ( $S_{\text{surf}}$ ) of mesopore, macropore and crystal external surface [33]. The pore size distribution (PSD) was determined according to the BJH-method [34], applied to the adsorption branches of the isotherm.

Diffuse reflectance (DRIFT) spectra of the samples were obtained from a Nicolet Nexus FTIR spectrometer, equipped with a diffuse reflectance attachment Smart Collector with KBr windows, a liquid nitrogen-cooled MCT/A detector and a Thermo Spectra-Tech heating control system. The whole compartment

holding the diffuse reflectance cell was flushed with dried  $\text{N}_2$  during experiment. Prior to the measurements, each sample was pretreated in situ at 673 K for 1.5 h under flow of dried  $\text{N}_2$   $40 \text{ ml min}^{-1}$  (STP). The spectra of the samples were collected at 523 K with a  $2 \text{ cm}^{-1}$  resolution and were subtracted from the background scanned at atmosphere.

$\text{NH}_3$ -TPD was carried out with a quartz reactor, a TCD detector and 200 mg sample with particle size 0.18–0.28 mm at atmospheric pressure. The system was quenched at 673 K for 1 h in a flow of He  $40 \text{ ml min}^{-1}$  (STP). After cooling to 373 K,  $\text{NH}_3$  was introduced by a pulsed injection with the He flow until saturation. The sample was quenched again at the temperature for 2 h to remove the excess  $\text{NH}_3$ . Desorption was then performed under the same He flow with a ramp of  $8 \text{ K min}^{-1}$  to 973 K.

The FTIR spectra of H-ZSM-5 adsorbed pyridine were collected in the transmission mode using a Bruker Vector 22 spectrometer. The samples were pressed into very thin self-supporting wafers with an optical diameter of 16 mm. The discs were mounted in a quartz IR cell equipped with a  $\text{CaF}_2$  window and a vacuum system. Prior to adsorption, the samples were pretreated in situ at 673 K for 1.5 h under evacuation, then cooled to 398 K where pyridine vapor was introduced into the cell for 0.5 h by volatilizing the pyridine at the volatilizer. The physically adsorbed pyridine was removed by evacuation for 1 h, then the sample was heated in vacuum for 2 h at 473 K, and a spectrum was recorded. The areas under the IR bands were calculated by OPUS software.

### 2.3. Catalytic reaction

The reaction was carried out at atmospheric pressure and 723 K by using 1.5 g catalyst with a particle size 0.18–0.28 mm in a stainless steel tubular reactor with a diameter of 10 mm. A mixture of acetaldehyde, 60% aqueous solution, and formaldehyde, 40% aqueous solution, was vaporized in a preheater at 523 K and mixed with ammonia and hydrogen, to make up a molar ratio of  $\text{C}_2\text{H}_4\text{O}:\text{CH}_2\text{O}:\text{NH}_3:\text{H}_2\text{O}:\text{H}_2 = 2:3:10:17:5$ . The GHSV was  $3131 \text{ h}^{-1}$ . The liquid product was collected using an ice-trap and analyzed with an Agilent 6890 GC equipped with a HP-5 column. The total yield of pyridine bases, i.e. pyridine, 3-picoline and 2-picoline, was used as the measure of the catalytic activity, which was calculated as  $\text{yield (\%)} = (\text{total C atoms in produced pyridine, 3-picoline and 2-picoline}) \times 100\% / (\text{total carbon atoms in feed})$ . The ratio between yield of pyridine and that of 3-picoline (P/3P) was used to discuss the selectivity.

## 3. Results

### 3.1. Structure and composition

The XRD patterns of H-ZSM-P, H-ZSM-At and H-ZSM-At-Ga show similar peak positions in Fig. 1, which indicates the H-ZSM-5 crystal structure was not destroyed during the alkaline and atom-planting treatment. However, H-ZSM-At has broadened peaks and lowered intensities than H-ZSM-P. Subsequent atom-planting treatment did not bring obvious farther change of peak intensities.

The  $^{27}\text{Al}$  NMR spectra of the samples are displayed in Fig. 2. The parent sample contained a stronger peak at around 50 ppm, which is ascribed to the tetrahedral framework aluminum ( $\text{Al}_f$ ), and weaker peak at around 0 ppm, which is due to the octahedral extraframework aluminum ( $\text{Al}_{\text{ef}}$ ) or amorphous  $\text{Al}_2\text{O}_3$  ( $\text{Al}_a$ ) [35–38]. After the alkaline treatment, the peak at around 50 ppm decreased and that at around 0 ppm increased. It means dealumination happened and the  $\text{Al}_{\text{ef}} + \text{Al}_a$  formatted at the same time. The signal at around 50 and 0 ppm was not obviously changed by

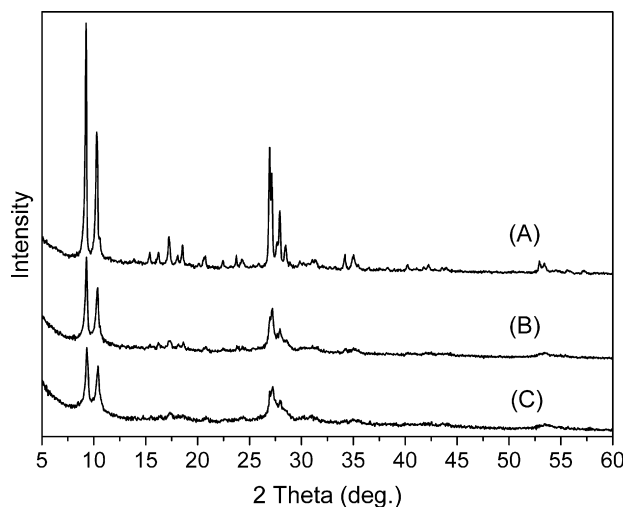


Fig. 1. X-ray diffraction patterns of H-ZSM-P (A), H-ZSM-At (B) and H-ZSM-At-Ga (C).

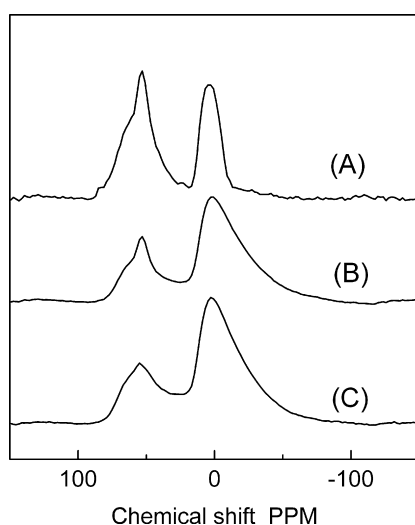


Fig. 2.  $^{27}\text{Al}$  NMR spectra of H-ZSM-P (A), H-ZSM-At (B) and H-ZSM-At-Ga (C).

further atom-planting treatment of the H-ZSM-At, which indicated that this treatment did not influence the  $\text{Al}_f$ ,  $\text{Al}_{ef}$  and  $\text{Al}_a$ . Moreover the EDX result shows that the atomic percentage of Ga in the H-ZSM-At-Ga is 0.43%.

The silicon atoms in the zeolite frameworks are tetrahedrally coordinated, resulting in five different silicon environments denoted as  $\text{Si}(n\text{Al})$ , where  $n$  ( $n=0, 1, 2, 3$  or  $4$ ) corresponds to the number of aluminum atoms in the second coordination sphere. The  $^{29}\text{Si}$  NMR is widely used for zeolites to determine the relative distributions of  $\text{Si}(n\text{Al})$  and to calculate their framework Si/Al ratios ( $(\text{Si}/\text{Al})_{\text{frame}}$ ). In H-ZSM-5 normally only two types of  $\text{Si}(n\text{Al})$ , i.e.  $\text{Si}(1\text{Al})$  and  $\text{Si}(0\text{Al})$ , are observed due to its high Si/Al ratio [39]. The chemical shift of  $\text{Si}(1\text{Al})$  is  $\sim -106$  ppm, and that of  $\text{Si}(0\text{Al})$  is  $\sim -112$  ppm [39]. For H-ZSM-5, the  $(\text{Si}/\text{Al})_{\text{frame}}$  can be calculated by using Eq. (1) [40,41].

$$\text{Si}/\text{Al} = S_{(\text{total})}/0.25S_{\text{Si}(1\text{Al})}, \text{ and } S_{(\text{total})} = S_{\text{Si}(0\text{Al})} + S_{\text{Si}(1\text{Al})} \quad (1)$$

$S_{\text{Si}(0\text{Al})}$  and  $S_{\text{Si}(1\text{Al})}$  are the areas of  $\text{Si}(0\text{Al})$  and  $\text{Si}(1\text{Al})$  signal peaks, respectively, which were calculated with deconvolution of the spectrum using a Gaussian method in this work. However, in the  $^{29}\text{Si}$  NMR spectra the signal of the silanol group ( $\text{SiOH}(\text{SiO})_3$ ) of

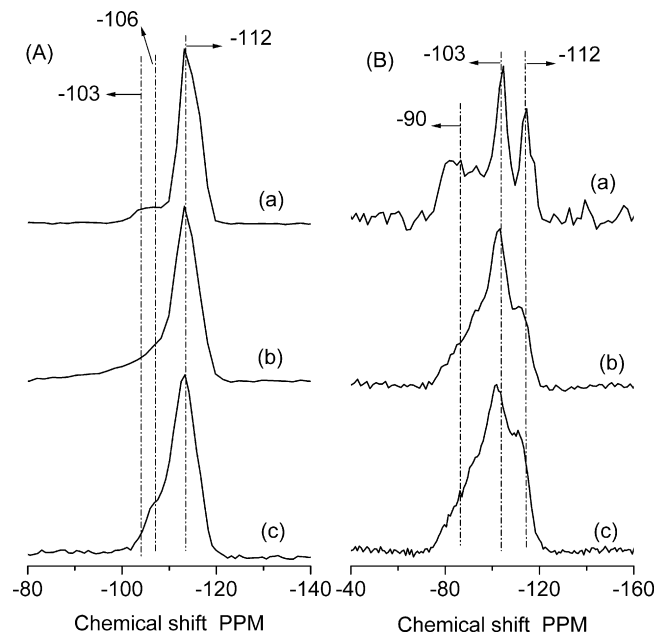


Fig. 3. (A)  $^{29}\text{Si}$  NMR spectra and (B)  $^1\text{H}-^{29}\text{Si}$  CP NMR spectra of H-ZSM-P (a), H-ZSM-At (b) and H-ZSM-At-Ga (c).

defect sites, which has a chemical shift as  $\sim -103$  ppm, is always a very weak peak and overlaps with that of  $\text{Si}(1\text{Al})$  [42,43]. Therefore, it is difficult to obtain qualitative information of  $\text{SiOH}(\text{SiO})_3$  from the  $^{29}\text{Si}$  NMR spectrum alone. Nevertheless the signal of  $\text{SiOH}(\text{SiO})_3$  can be enhanced strongly by  $^1\text{H}-^{29}\text{Si}$  CP technique. The  $^1\text{H}-^{29}\text{Si}$  CP spectra can provide qualitative information about the  $\text{SiOH}(\text{SiO})_3$  on the defect sites of ZSM-5 zeolite by comparing with the  $^{29}\text{Si}$  NMR spectrum [42,43]. Hence, the  $^{29}\text{Si}$  NMR spectra of the samples without CP and with CP are displayed in Fig. 3. The H-ZSM-P exhibits in its non-CP spectrum (Fig. 3(A)(a)) a sharp peak around  $\sim -112$  ppm, which is attributed to the  $\text{Si}(0\text{Al})$ , and a broad peak between  $-103$  and  $\sim -106$  ppm, which is corresponding to the overlap of the  $\text{SiOH}(\text{SiO})_3$  and  $\text{Si}(1\text{Al})$ . The CP spectrum of H-ZSM-P (Fig. 3(B)(a)) shows a stronger signal at  $\sim -103$  ppm than that at  $\sim -112$  and  $\sim -106$  ppm, because the dipolar coupling effect between proton with silicon of  $\text{SiOH}(\text{SiO})_3$  is stronger than that of  $\text{Si}(0\text{Al})$  and  $\text{Si}(1\text{Al})$ . The poor signal-to-noise ratio of this spectrum indicates the concentration of  $\text{SiOH}(\text{SiO})_3$  on the H-ZSM-P is very low. The weak peak around  $\sim -90$  ppm is ascribed to the small amount of  $\text{Si}(\text{OH})_2(\text{OSi})_2$  in this spectrum [43,44]. In the non-CP spectra (Fig. 3(A)), after alkaline treatment the peak intensity between  $-103$  and  $\sim -106$  ppm of the H-ZSM-At is stronger than that of H-ZSM-P, this broad peak become a shoulder of the peak around  $-112$  ppm. After subsequent atom-planting the  $-103$  ppm peak intensity decreases and the  $-106$  ppm peak intensity increases in comparison of H-ZSM-At-Ga and H-ZSM-At. However the intensity of the peak at  $-112$  ppm almost does not change after alkaline and subsequent atom-planting treatments. The  $(\text{Si}/\text{Al})_{\text{frame}}$  was calculated according to Eq. (1) and illustrated in Table 1. For the H-ZSM-At-Ga the calculated  $(\text{Si}/\text{Al})_{\text{frame}}$  is nominal because it contains Ga cations. In the CP spectra (Fig. 3(B)), after the alkaline treatment the  $-103$  ppm peak intensity of H-ZSM-At is much stronger than that of the H-ZSM-P, which indicates the concentration of the  $\text{SiOH}(\text{SiO})_3$  increased obviously. After the subsequent atom-planting treatment the ratio of  $-103$  ppm peak intensity to  $-112$  ppm peak intensity in the CP spectrum of H-ZSM-At-Ga is lower than that in H-ZSM-At. This result demonstrates that the concentration of the  $\text{SiOH}(\text{SiO})_3$  decreased after atom-planting treatment.

**Table 1**  
The textural properties of different catalysts

Sample	(Si/Al) <sub>frame</sub> <sup>a</sup>	S <sub>BET</sub> (×10 <sup>-2</sup> m <sup>2</sup> /g)	v <sub>total</sub> (×10 cm <sup>3</sup> /g)	v <sub>microp</sub> (×10 <sup>2</sup> cm <sup>3</sup> /g)	v <sub>mesop</sub> (×10 cm <sup>3</sup> /g) <sup>b</sup>	S <sub>surf</sub> (×10 <sup>-2</sup> m <sup>2</sup> /g)
H-ZSM-P	35	3.27	2.42	9.5	1.47	1.44
H-ZSM-At	12	3.33	4.25	5.3	3.72	2.32
H-ZSM-At-Ga	9 <sup>c</sup>	3.24	4.17	5.3	3.64	2.23

<sup>a</sup> Calculated from <sup>29</sup>Si NMR.

<sup>b</sup> v<sub>mesop</sub> = v<sub>total</sub> - v<sub>microp</sub>.

<sup>c</sup> (Si/(Al+Ga))<sub>frame</sub>.

### 3.2. Pore structure

The N<sub>2</sub> adsorption–desorption isotherms of the samples are depicted in Fig. 4. The isotherm of H-ZSM-P exhibits a type I curve as a result of its microporous nature. A very small H2-type hysteresis loop is obvious, which suggests that some mesopores exist in H-ZSM-P. After alkaline treatment the isotherm is transformed from type I to type IV. The uptake of N<sub>2</sub> at higher relative pressures was enhanced. However the isotherms of H-ZSM-At-Ga are similar to that of H-ZSM-At.

The PSD curves calculated by the BJH model with the data of the adsorption branch are illustrated in Fig. 5. The pore with diameters between 1 and 10 nm is shown in H-ZSM-P, while a broad peak in 1–100 nm is developed in H-ZSM-At. The curve of H-ZSM-At-Ga is similar to that of H-ZSM-At. Table 1 summarizes the S<sub>BET</sub>, v<sub>total</sub>, v<sub>microp</sub>, mesopore volume (v<sub>mesop</sub>), and S<sub>surf</sub>. The BET model for the calculation of materials with micropores can be reasonably used for comparison purpose [23]. It can be seen from the data in Table 1 that after alkaline treatment the S<sub>BET</sub> and v<sub>total</sub> increased. The v<sub>mesop</sub> and S<sub>surf</sub> increased, while the v<sub>microp</sub> volume decreased. After subsequent atom-planting treatment, the S<sub>BET</sub>, v<sub>total</sub>, S<sub>surf</sub>, v<sub>microp</sub> and v<sub>mesop</sub> of H-ZSM-At-Ga changed little compared to H-ZSM-At.

### 3.3. Acidity

The DRIFT spectra in the hydroxyl stretching region for the H-ZSM-P, H-ZSM-At and H-ZSM-At-Ga are depicted in Fig. 6. The parent sample H-ZSM-P shows two bands, the band at about 3610 cm<sup>-1</sup> is attributed to the framework bridged hydroxyl groups (Al(OH)Si), while that at about 3700–3740 cm<sup>-1</sup> is associated with SiOH(SiO)<sub>3</sub>, i.e. isolated silanol groups at the external surface, free silanol and internal silanol groups of defect sites [31,45–48]. After alkaline treatment the intensity of the band around 3700–3740 cm<sup>-1</sup> rises a lot indicating the increases of SiOH(SiO)<sub>3</sub> concentration. A broad band between 3610 and 3660 cm<sup>-1</sup> appears synchronously, which may be the result of overlapping of the band of Al(OH)Si around 3610 cm<sup>-1</sup> and the band around 3660 cm<sup>-1</sup> assigned to Al<sub>ef</sub> [29]. Subsequent atom-planting treatment resulted in the reduction of intensity of the band around 3700–3740 cm<sup>-1</sup>, which means the concentration of the SiOH(SiO)<sub>3</sub> decreased. Moreover, the band around 3610–3660 cm<sup>-1</sup> was splitted into two bands at ~3660 cm<sup>-1</sup> and ~3620 cm<sup>-1</sup> by this treatment. In the bridged hydroxyl groups stretching region of 3610–3620 cm<sup>-1</sup>, the atom-planting caused the hydroxyl group band of H-ZSM-At-Ga shifted to a higher wave number as compared to that of H-ZSM-P which only contained trivalent Al cations in the framework.

The NH<sub>3</sub>-TPD curves of the samples are depicted in Fig. 7. The curves have two peaks corresponding to two kinds of acid sites, i.e. the weak sites associated with the TPD peak at around 450–625 K, and the strong sites related to the peak at around 650–750 K. After alkaline treatment the total amount of acid sites increased, and the

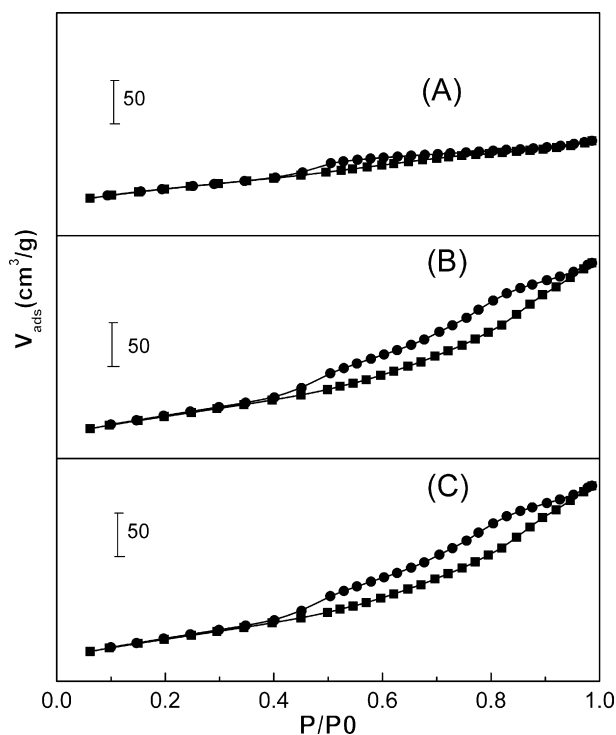


**Fig. 4.** The N<sub>2</sub>-adsorption (●) and desorption (■) isotherms at 77 K. H-ZSM-P (A), H-ZSM-At (B) and H-ZSM-At-Ga (C).

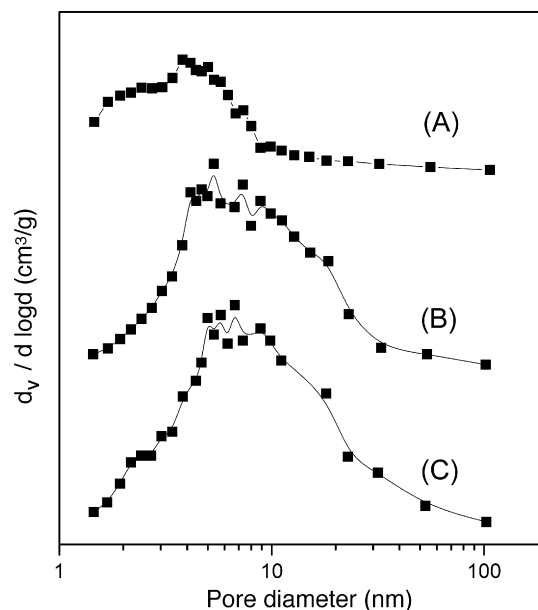


**Fig. 5.** BJH pore-size distributions derived from the adsorption branch H-ZSM-P (A), H-ZSM-At (B) and H-ZSM-At-Ga (C).

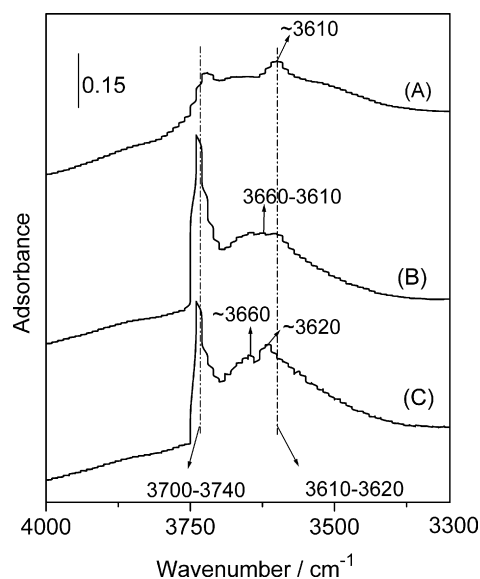


**Fig. 6.** FTIR spectra of H-ZSM-P (A), H-ZSM-At (B), H-ZSM-At-Ga (C) in the hydroxyl group stretching region ( $4000\text{--}3300\text{ cm}^{-1}$ ).

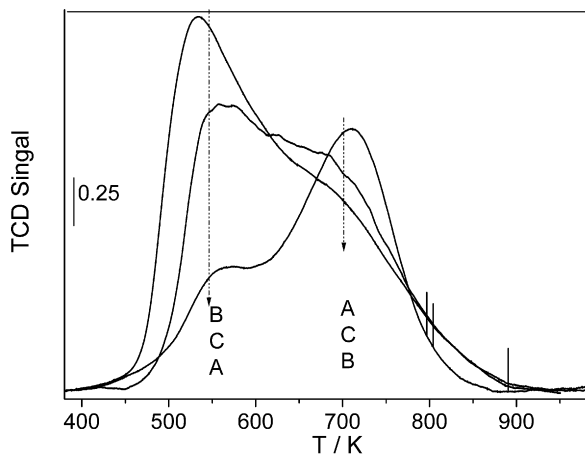


**Fig. 7.**  $\text{NH}_3$ -TPD curves of H-ZSM-5 (A), H-ZSM-5-At (B) and H-ZSM-5-At-Ga (C).

amount of strong sites decreased, while that of the weak sites increased. Subsequent atom-planting caused the decrease of the total amount of acid sites, increase of the amount of strong sites and decrease of the amount of weak sites.

The Brønsted (B) and Lewis (L) acid sites on the samples can be discriminated by the IR spectra after adsorption of pyridine as shown in Fig. 8. It shows the adsorption bands of pyridine coordinated to L sites at  $\sim 1450\text{ cm}^{-1}$  and adsorption bands of pyridinium ion on B sites at  $\sim 1550\text{ cm}^{-1}$  [49,50]. The areas under the IR bands at  $\sim 1450\text{ cm}^{-1}$  and  $\sim 1540\text{ cm}^{-1}$  contain the information of the relative ratio of the L and B sites. The L/B ratio (area of  $\sim 1450\text{ cm}^{-1}$  band/area of  $\sim 1540\text{ cm}^{-1}$  band) of H-ZSM-P was 6.90. After alkaline treatment the L/B ratio of H-ZSM-At reached 13.2. Subsequent atom-planting resulted in the L/B ratio of H-ZSM-At-Ga reduced to 7.5.

### 3.4. Catalytic performance

Figs. 9–11 depicts the yield of total pyridine bases, pyridine and 3-picoline as a function of time on stream (TOS), respectively. The alkaline treatment almost did not change the initial yield (IY) of pyridine bases in comparison of H-ZSM-At and H-ZSM-P, while the subsequent atom-planting treatment increased the IY of pyridine

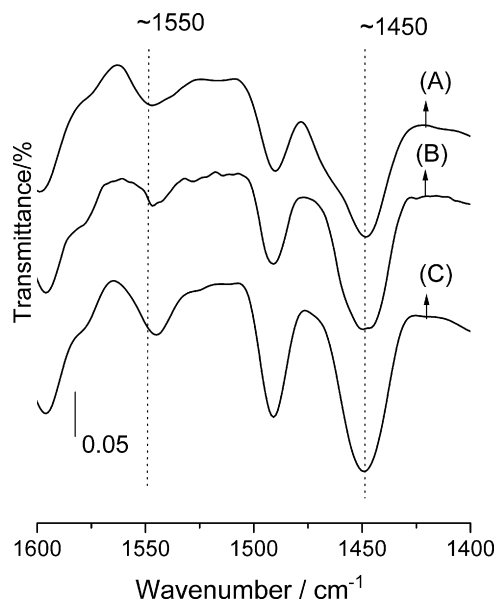


**Fig. 8.** FTIR spectra obtained after adsorption of pyridine over H-ZSM-P (A), H-ZSM-At (B) and H-ZSM-At-Ga (C) at 473 K.

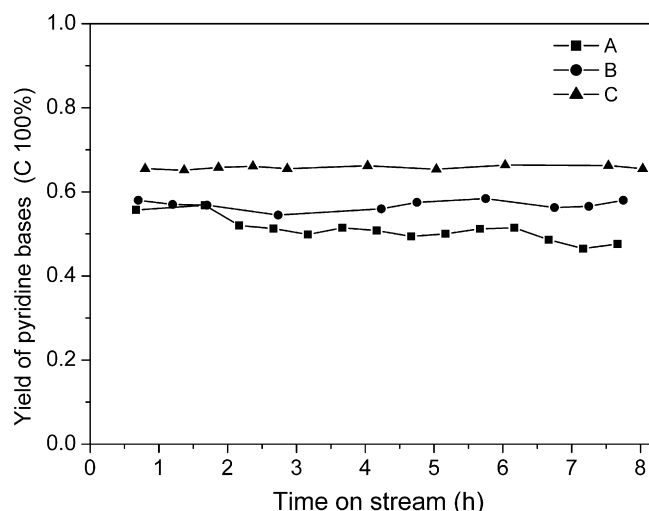


**Fig. 9.** Yield of pyridine bases versus TOS. H-ZSM-P (A), H-ZSM-At (B) and H-ZSM-At-Ga (C).

bases. The IY of pyridine increased gradually after alkaline treatment and subsequent atom-planting treatment. Alkaline treatment decreased the IY of 3-picoline in comparison of H-ZSM-At and H-ZSM-P, but subsequent atom-planting treatment increased the IY of 3-picoline of H-ZSM-At-Ga as compared to H-ZSM-At. The stability of H-ZSM-At and H-ZSM-At-Ga was superior to that of H-ZSM-P for pyridine and picolines synthesis.

Fig. 12 depicts the change of P/3P ratios as a function of TOS. The initial P/3P ratio exhibited an increase in H-ZSM-At as compared to H-ZSM-P and a decrease in H-ZSM-At-Ga as compared to H-ZSM-At. The P/3P ratios of H-ZSM-P increased with the increase of TOS, while those of H-ZSM-At and H-ZSM-At-Ga were stable.

## 4. Discussion

### 4.1. Phase composition

After alkaline treatment, the XRD pattern confirms the preservation of ZSM-5 structure in the sample, but with a much

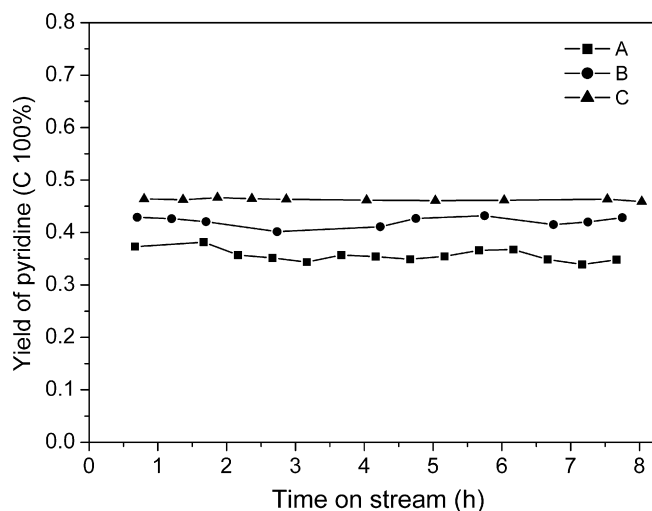


Fig. 10. Yield of pyridine versus TOS. H-ZSM-P (A), H-ZSM-At (B) and H-ZSM-At-Ga (C).

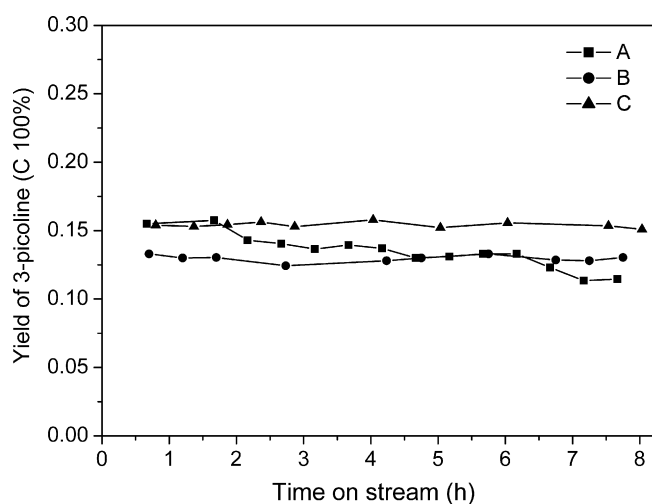


Fig. 11. Yield of 3-picoline versus TOS. H-ZSM-P (A), H-ZSM-At (B) and H-ZSM-At-Ga (C).

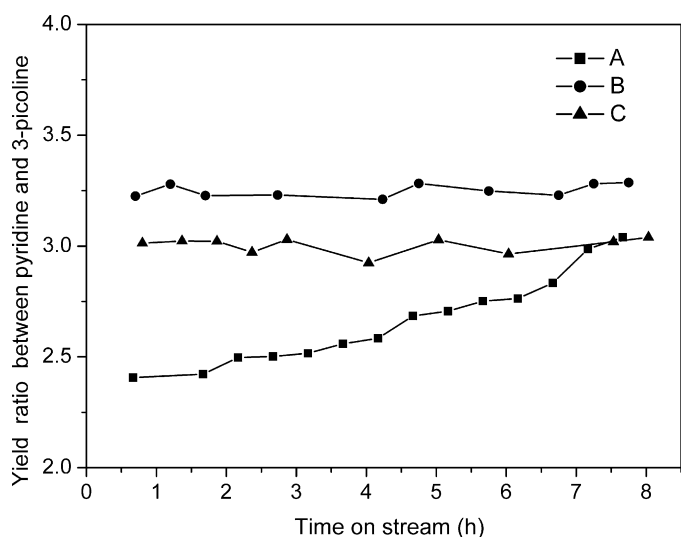
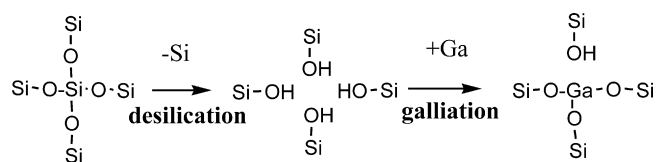


Fig. 12. Pyridine/3-picoline yield ratio versus TOS. H-ZSM-P (A), H-ZSM-At (B) and H-ZSM-At-Ga (C).



Scheme 1.

smaller nominal crystallite size or a reduced crystallinity, as the peaks were weakened. The decreased amount of  $Al_f$  and  $(Si/Al)_{frame}$  (Figs. 2 and 3(A)) indicated that the major function of alkaline treatment is desilication. The dislodgement of one Si on the framework can form four internal silanol groups, i.e. the defect sites as shown in Scheme 1. So the concentration of silanol groups increased (Fig. 3(B) and Fig. 6). The decreased amount of  $Al_f$  and largely increased amount of  $Al_{ef}$  and  $Al_a$  (Fig. 2) suggest that dealumination happened simultaneously and a part of the  $Al_f$  transformed into  $Al_{ef}$  and  $Al_a$  during the alkaline treatment. It is likely that the alkaline corrosion does start preferentially from the silicon position and the aluminum in the detached part was finally transformed from tetrahedrally coordinated to octahedrally coordinated ones. That supposition is in consistency with the results of Lietz et al. [19] and Groen et al. [24].

After subsequent atom-planting treatment the H-ZSM-At-Ga not only maintained the ZSM-5 structure but also contained the Ga cations. The  $^{27}Al$  NMR (Fig. 2) shows that this treatment does not influence the  $Al_f$ . So the increased nominal  $Si/Al_{frame}$  (Table 1 and Fig. 3(A)) may be a result of introducing Ga into the zeolite framework and generating  $Si(1Ga)$ , because the  $Si(1Ga)$  gives a contribution to the signal close to that of  $Si(1Al)$  in the non-CP  $^{29}Si$  NMR spectra [51]. The incorporation of trivalent Ga cations into the tetrahedral framework forms acidic bridged hydroxyl groups  $Si(OH)Ga$  corresponding to the B acid sites. As the band of  $Si(OH)Al$  and  $Si(OH)Ga$  groups in MFI structure is generally observed at around  $3610$  and  $3620\text{ cm}^{-1}$ , respectively [29,52]. Therefore, the fact that the bridged hydroxyl groups band shifted to higher wavenumber after successive treatment (Fig. 6) indicated that the band around  $3620\text{ cm}^{-1}$  of H-ZSM-At-Ga may be the overlapped band of  $Si(OH)Ga$  and  $Si(OH)Al$ . So the incorporation of the Ga cations into the MFI framework has been further confirmed by the IR spectra. The decreased concentration of the silanol groups in IR spectra (Fig. 6) agrees well with the result of  $^1H$ - $^{29}Si$  NMR result (Fig. 3(B)). These results are consistent with those of Yashima et al. [29,30], Yashima [30] and Ei-Malki et al. [31]. They proposed that the Ga cations can be built into the zeolite framework through the reaction between  $GaCl_3$  and silanol groups on the defect sites of zeolite, as shown in Scheme 1. So the defect sites generated by desilication provided active sites for the galliation. After the atom-planting reaction the silanol groups were consumed, while the bridged hydroxyl groups were developed.

#### 4.2. Pore structure

A few mesopores existing in H-ZSM-P may be the inter-crystal mesopores between the ZSM-5 and  $Al_a$  in the samples [20,53]. The shape of the hysteresis loop of the isotherms changes after alkaline treatment, which means a large number of meso- or macropore formed, and the PSD curves confirm that result. Hence, the treatment here is very effective for creating extra-pores in H-ZSM-5. Moreover the  $v_{microp}$  was still large in H-ZSM-At, which indicates that the micropores were only partly destroyed by alkaline treatment. After subsequent atom-planting treatment, the H-ZSM-At-Ga still contained the hierarchical pore structure.

### 4.3. The acidity

After alkaline treatment, three explanations can be considered for the change of the acid strength distribution (Fig. 7). One of them is that a large number of developed silanol groups during desilication can increase the acid amount, especially for weak acid sites. The other interpretation is that the decreased  $(\text{Si}/\text{Al})_{\text{frame}}$  can lead to an increase of the amount of weak acid sites and a decrease of the amount of strong acid sites, which is in agreement with the results reported by Ogura et al. [22]. The third reason is that the formed  $\text{Al}_a$  and  $\text{Al}_{\text{ef}}$  during alkaline treatment causes the acid strength distribution change. Kim et al. [54] found that mixing of  $\text{Na}(\text{H})\text{-ZSM-5}$  with  $\gamma\text{-Al}_2\text{O}_3$  gave rise to a higher intensity of  $\text{NH}_3\text{-TPD}$  peak in low temperature range and a lower intensity of the peak in high temperature range. The subsequent atom-planting treatment consumed four silanol groups and generated only one  $\text{Si}(\text{OH})\text{Ga}$  group. The acid strength of the bridged hydroxyl groups  $\text{Si}(\text{OH})\text{Ga}$  is stronger than the silanol groups. So the acid strength distribution in Fig. 7 has a corresponding change after atom-planting treatment.

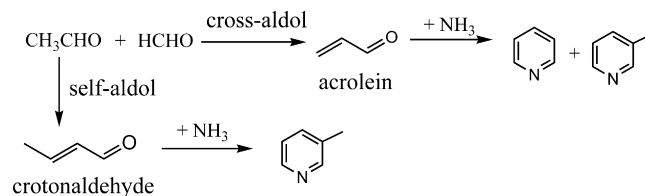
From the results of our IR studies in Fig. 8, it can be proposed that the alkaline treatment dislodged  $\text{Al}_f$ , which resulted in the decrease of B sites in the zeolite framework and the formed  $\text{Al}_{\text{ef}}$  and  $\text{Al}_a$  may act as L sites [54,55]. Subsequent atom-planting generated  $\text{Si}(\text{OH})\text{Ga}$  groups responsible for B sites, which causes the L/B ratio decrease.

### 4.4. The catalytic performance

The deactivation of ZSM-5 in the reaction is attributed to the coke formation which covers the acid sites and blocks the micropores. After alkaline treatment a large number of secondary meso- and macropores were introduced, those can weaken the diffusion limitation of the intermediates and products in the micropores, and moderate the pore coverage effect of coke and its precursors. This proposition has been confirmed by the catalytic performance results (Figs. 9–11).

The large increase of total acid amount after alkaline treatment did not increase the IY of pyridine bases. That may be because that most of the increased acid amount in the H-ZSM-At is attributed to the formed silanol groups, which is the weak acid sites and is not sensitive for the pyridine bases synthesis in the reaction. The subsequent galliation generated the B acid sites of bridged hydroxyl groups  $\text{Si}(\text{OH})\text{Ga}$ , which is strong acid sites and is more active for pyridine bases synthesis. So the IY of pyridine bases of H-ZSM-At-Ga increased as compared to H-ZSM-At.

Both B and L acid sites took part in the Chichibiabin reaction but may involve different mechanism [10]. Singh et al. [16] proposed a mechanism for pyridine bases synthesis from formaldehyde, acetaldehyde and ammonia: the cross-aldol condensation of formaldehyde and acetaldehyde happens and produces an intermediate acrolein, and the self-aldol condensation of acetaldehyde occurs and produces another intermediate crotonaldehyde. Then acrolein reacts with ammonia and produces both pyridine and 3-picoline, while crotonaldehyde reacts with ammonia and produces only 3-picoline. The mechanism can be written as Scheme 2. Dumitriu et al. [56] investigated the aldol condensation of formaldehyde and acetaldehyde over MFI zeolites. They found that on B sites acetaldehyde is favored than formaldehyde to form a cation and react with the enol form of the acetaldehyde because acetaldehyde has higher electronic density at the oxygen atom than formaldehyde, so the crotonaldehyde is favored over the acrolein. They postulated also that L sites may favor the formation of formaldehyde cation or that the L sites can stabilize the enol form of the acetaldehyde, shift the keto–



Scheme 2.

enol equilibrium of the acetaldehyde towards the enol form, decrease the amount of acetaldehyde cation activated by B sites and increase the concentration of activated formaldehyde cation by B sites. So the L sites favor acrolein formation and cross-condensation is enhanced to same extent. The parent sample H-ZSM-P contained both B and L sites and produced the pyridine and 3-picoline. After alkaline treatment, the ratio L/B increased. According to the above mechanism acrolein should be enhanced, and at same time crotonaldehyde be depressed. This would lead to an increase of pyridine yield and a decrease of 3-picoline yield. Here, the experimental results are in consistency to such reasoning. The P/3P of the H-ZSM-At-Ga was lower than that of H-ZSM-At because the  $\text{Si}(\text{OH})\text{Ga}$  generated and L/B ratio decreased after subsequent atom-planting treatment.

The fact that the P/3P increased with the increase of TOS for the H-ZSM-P reflects that the coke-induced selectivity change. The amounts of the deposited carbonaceous species increased with the increase of TOS. This induced a gradually pore blockage. Then larger molecule intermediate crotonaldehyde and product 3-picoline is unfavorable over the smaller molecule intermediate acrolein and product pyridine. Due to the sample H-ZSM-At and H-ZSM-At-Ga have improved pore system, and the pore blockage of this sample was much less severe than the untreated sample, therefore its P/3P was much more stable with the TOS than the untreated sample.

## 5. Conclusions

After alkaline treatment, the treated sample retained the ZSM-5 structure and micropores. The major function of alkaline treatment was desilication, a slight dealumination happened simultaneously. The desilication generated a large number of silanol groups of defect sites, meso- and macropores, while dealumination dislodged the  $\text{Al}_f$  to form  $\text{Al}_a$  and  $\text{Al}_{\text{ef}}$ . The generation of silanol groups, decrease of  $(\text{Si}/\text{Al})_{\text{frame}}$  and formation of  $\text{Al}_a$  and  $\text{Al}_{\text{ef}}$  increased the amount of weak acid sites, decreased the amount of strong acid sites and increased the L/B ratio. The tailored sample contained hierarchical pore structure. During the subsequent atom-planting treatment, the consumption of silanol groups and generation of  $\text{Si}(\text{OH})\text{Ga}$  caused the decrease of weak acid sites, the increase of the strong acid sites and the decrease of L/B ratio. While this treatment made little impact on the hierarchical pore structure.

The alkaline treatment improved the stability of the catalyst effectively, which is ascribed to the introduced secondary pores which depressed the coke formation and diminished the blockage effect of the carbonaceous species. After alkaline treatment the increased amount of silanol groups and weak acid sites did not change the pyridine bases IY, while the increase of the P/3P ratio is attributed to the increase of L/B ratio. After subsequent atom-planting treatment the generated bridged hydroxyl groups  $\text{Si}(\text{OH})\text{Ga}$ , which has acid strength stronger than that of the silanol groups, improved the pyridine bases IY, while the decreases of L/B ratio caused the decreases of P/3P ratio. An increase of P/3P with the increase of TOS was observed during the reaction for the parent samples, but the two tailored samples exhibited the most

stable P/3P ratio. This was explained with the coke-induced selectivity change effect.

### Acknowledgements

This work has been supported by the Natural Science Foundation of China under contract numbers 20425619. The work has been also supported by the Program of Introducing Talents to the University Disciplines under file number B06006, the Program for Changjiang Scholars and Innovative Research Teams in Universities under file number IRT 0641 and the Youths Science Foundation of Wuhan Institute of Technology under file number Q200901.

### References

- [1] A.E. Chichibabin, *J. Prakt. Chem.* 107 (1924) 154–158.
- [2] A.E. Cislak, W.R. Wheeler, US Patent 2,744,904 (1956).
- [3] J.R. Calvin, R.D. Davis, C.H. Mcateer, *Appl. Catal. A: Gen.* 285 (2005) 1–23.
- [4] G.I. Goe, R.D. Davis, US Patent 5,218,122 (1993).
- [5] G.K. Chitnis, J.A. Kowalski, J.P. Williams, US Patent 5,994,550 (1999).
- [6] J.I. Darragh, US Patent 4,089,863 (1978).
- [7] W. Hoelderich, N. Goetz, US Patent 5,079,367 (1992).
- [8] S. Shimizu, N. Abe, EP Patent 0,382,543A (1990).
- [9] S. Shimizu, N. Abe, A. Iguchi, M. Dohba, S. Hiroshi, K. Hirose, *Micropor. Mesopor. Mater.* 21 (1998) 447–451.
- [10] S. Shimizu, N. Abe, A. Iguchi, H. Sato, *Catal. Surv. Jpn.* 2 (1998) 71–76.
- [11] R. Ramachandra Rao, S.J. Kulkarni, M. Subrahmanyam, A.V. Rama Rao, *React. Kinet. Catal. Lett.* 56 (1995) 301–309.
- [12] Y.M. Liu, H.Q. Yang, F. Jin, Y. Zhang, Y.D. Li, *Chem. Eng. J.* 136 (2008) 282–287.
- [13] K.R.S.K. Reddy, I. Sreedhar, K.V. Raghavan, *Appl. Catal. A: Gen.* 339 (2008) 15–20.
- [14] K. Iwamoto, T. Shoji, US Patent 6,281,262B1 (2001).
- [15] A. Agarwal, P.K. Verma, K.S. Singh, US Patent 2,005,013,123,5A1 (2005).
- [16] B. Singh, S.K. Roy, K.P. Sharma, T.K. Goswami, *J. Chem. Technol. Biotechnol.* 71 (1998) 246–252.
- [17] J. Kärger, D.M. Ruthven, *Diffusion in Zeolites and Other Microporous Materials*, Wiley, New York, 1992.
- [18] Y. Tao, H. Kanoh, K. Kaneko, *Adsorption* 12 (2006) 309–316.
- [19] G. Lietz, K.H. Schnabel, C. Peuker, T. Gross, W. Storek, J. Völter, *J. Catal.* 148 (1994) 562–568.
- [20] A. Čížmek, B. Subotić, R. Aiello, F. Crea, A. Nastro, C. Tuoto, A. Čížmek, B. Subotić, I. Šmit, A. Tonejc, R. Aiello, F. Crea, A. Nastro, *Microporous. Mater.* 4 (1995) 159–168.
- [21] T.S. Le, R. Le Van Mao, *Micropor. Mesopor. Mater.* 34 (2000) 93–97.
- [22] M. Ogura, S. Shinomiya, J. Tateno, Y. Nara, M. Nomura, E. Kikuchi, M. Matsukata, *Appl. Catal. A: Gen.* 219 (2001) 33–43.
- [23] J.C. Groen, L.A.A. Peffer, J.A. Moulijn, J. Pérez-Ramírez, *Micropor. Mesopor. Mater.* 69 (2004) 29–34.
- [24] J.C. Groen, L.A.A. Peffer, J.A. Moulijn, J. Pérez-Ramírez, *Chem. Eur. J.* 11 (2005) 4983–4994.
- [25] J.C. Groen, L.A.A. Peffer, J.A. Moulijn, J. Pérez-Ramírez, *Colloid Surface A* 241 (2004) 53–58.
- [26] K. Yamagishi, S. Namba, T. Yashima, *J. Catal.* 121 (1990) 47–55.
- [27] T. Yashima, K. Yamagishi, S. Namba, *Stud. Surf. Sci. Catal.* 60 (1991) 171–178.
- [28] K. Yamagishi, S. Namba, T. Yashima, *J. Phys. Chem.* 95 (1991) 872–877.
- [29] K. Yamagishi, S. Namba, T. Yashima, *Bull. Chem. Soc. Jpn.* 64 (1991) 949–953.
- [30] T. Yashima, *Catal. Surv. Jpn.* 2 (1998) 121–132.
- [31] E.I.-M. El-Malki, R.A. van Santen, W.M.H. Sachtler, *J. Phys. Chem. B* 10 (1999) 4611–4622.
- [32] S. Brunauer, P.H. Emmett, E. Teller, *J. Am. Chem. Soc.* 60 (1938) 309–319.
- [33] B.C. Lippens, J.H. de Boer, *J. Catal.* 4 (1965) 319–323.
- [34] E.P. Barret, L.G. Joyner, P.P. Halenda, *J. Am. Chem. Soc.* 73 (1951) 373–380.
- [35] M. Sawa, M. Niva, Y. Murakami, *Zeolite* 10 (1990) 532–538.
- [36] C.A. Fyfe, G.C. Gobbi, J.S. Hartman, J. Klinowski, J.M. Thomas, *J. Phys. Chem.* 86 (1982) 1247–1250.
- [37] J. Klinowski, J.M. Thomas, C.A. Fyfe, G.C. Gobbi, J.S. Hartman, *Inorg. Chem.* 22 (1983) 63–66.
- [38] M.W. Kasture, P.S. Niphadkar, V.V. Bokade, P.N. Joshi, *Catal. Commun.* 8 (2007) 1003–1008.
- [39] G. Engelhardt, B. Fahlke, M. Maegi, E. Lippmaa, *Z. Phys. Chem. (Leipzig)* 266 (1985) 239–242.
- [40] G. Engelhardt, D. Michel, *High-Resolution Solid-State NMR of Silicates and Zeolites*, Wiley, Chichester, 1987.
- [41] J.B. Nagy, Z. Gabelica, E.G. Derouane, P.A. Jacobs, *Chem. Lett.* 11 (1982) 2003–2006.
- [42] J.B. Nagy, Z. Gabelica, E.G. Derouane, *Chem. Lett.* 11 (1982) 1105–1108.
- [43] G. Boxhoorn, A.G.T.G. Kortbeek, G.R. Hays, N.C.M. Alma, *Zeolites* 4 (1984) 15–21.
- [44] G.E. Maciel, D.W. Sindorf, *J. Am. Chem. Soc.* 102 (1980) 7606–7607.
- [45] A. Maiganen, E.G. Derouane, J.B. Nagy, *Appl. Surf. Sci.* 75 (1994) 204–212.
- [46] R. Buzzoni, S. Bordiga, G. Ricchiardi, C. Lamberti, *Langmuir* 12 (1996) 930–940.
- [47] A. Ungureanu, T.V. Hoang, D. Trongon, *Appl. Catal. A: Gen.* 294 (2005) 92–105.
- [48] P. Wu, T. Komatsu, T. Yashima, *J. Phys. Chem.* 99 (1995) 10923–10931.
- [49] J.C. Védrine, A. Auroux, V. Bolis, P. Dejaifve, C. Naccache, P. Wierzychowski, E.G. Derouane, J.B. Nagy, J.P. Gilson, J.H.C. van Hooff, J.P. van den Berg, *J. Catal.* 59 (1979) 248–262.
- [50] A. Maijanen, E.G. Derouane, J.B. Nagy, *Appl. Surf. Sci.* 75 (1994) 204–212.
- [51] C.R. Bayense, A.P.M. Kentgens, J.W. De Haan, L.J.M. Van de Ven, J.H.C. Van Hooff, *J. Phys. Chem.* 96 (1992) 775–782.
- [52] C.T.-W. Chu, C.D. Chang, *J. Phys. Chem.* 89 (1985) 1569–1571.
- [53] R. Le Van Mao, *Micropor. Mesopor. Mater.* 28 (1999) 9–17.
- [54] S.D. Kim, S.C. Baek, Y.J. Lee, K.W. Jun, M.J. Kim, I.S. Yoo, *Appl. Catal. A: Gen.* 309 (2006) 139–143.
- [55] J.L. Motz, H. Heinichen, W.F. Hölderich, *Stud. Surf. Sci. Catal.* 105 (1997) 1053–1060.
- [56] E. Dumitriu, V. Hulea, I. Fechete, A. Aurous, J.F. Lacaze, C. Guimon, *Micropor. Mesopor. Mater.* 43 (2001) 341–359.